Radial polarization interferometer

Gilad M. Lerman and Uriel Levy*

Department of Applied Physics, The Benin School of Engineering and Computer Science, The Center for Nanoscience and Nanotechnology, The Hebrew University of Jerusalem, Jerusalem, 91904, Israel
**ulevy@cc.huji.ac.il*

Abstract: We propose and demonstrate a new interferometric approach in which a uniform phase difference between the arms of the interferometer manifests itself as spatially varying intensity distribution. The approach is based on interfering two orthogonal spatially varying vector fields, the radially and azimuthally polarized beams, and measuring the projection of the obtained field on an analyzer. This method provides additional spatial information that can be used to improve the smallest detectable phase change as compared with a conventional Michelson interferometer.

OCIS codes: (260.5430) Polarization; (120.3180) Interferometry; (120.5050) Phase measurement

References and links

1. R. Dorn, S. Quabis, and G. Leuchs, "Sharper focus for a radially polarized light beam," Phys. Rev. Lett. **91**(23), 233901 (2003).
2. Q. Zhan, "Cylindrical vector beams: from mathematical concepts to applications," Adv. Opt. Photon. **1**(1), 1–57 (2009).
3. U. Levy, C. H. Tsai, L. Pang, and Y. Fainman, "Engineering space-variant inhomogeneous media for polarization control," Opt. Lett. **29**(15), 1718–1720 (2004).
4. Y. Kozawa, and S. Sato, "Focusing property of a double-ring-shaped radially polarized beam," Opt. Lett. **31**(6), 820–822 (2006).
5. G. M. Lerman, and U. Levy, "Effect of radial polarization and apodization on spot size under tight focusing conditions," Opt. Express **16**(7), 4567–4581 (2008).
6. B. Hao, and J. Leger, "Experimental measurement of longitudinal component in the vicinity of focused radially polarized beam," Opt. Express **15**(6), 3550–3556 (2007).
7. K. S. Youngworth, and T. G. Brown, "Focusing of high numerical aperture cylindrical-vector beams," Opt. Express **7**(2), 77–87 (2000).
8. F. Flossmann, U. T. Schwarz, M. Maier, and M. R. Dennis, "Polarization singularities from unfolding an optical vortex through a birefringent crystal," Phys. Rev. Lett. **95**(25), 253901 (2005).
9. J. L. Flores, J. A. Ferrari, and C. D. Perciante, "Faraday current sensor using space-variant analyzers," Opt. Eng. **47**(12), 123603 (2008).
10. J. A. Ferrari, W. Dultz, H. Schmitzer, and E. Frins, "Achromatic wavefront forming with space-variant polarizers: Application to phase singularities and light focusing," Phys. Rev. A **76**(5), 053815 (2007).
11. N. Bokor, and N. Davidson, "Toward a spherical spot distribution with 4pi focusing of radially polarized light," Opt. Lett. **29**(17), 1968–1970 (2004).
12. Q. Zhan, and J. R. Leger, "Interferometric measurement of the geometric phase in space-variant polarization manipulations", Opt. Comm., **213**," Issues **4-6**, 241–245 (2002).
13. I. Nishiyama, N. Yoshida, Y. Otani, and N. Umeda, "Single-shot birefringence measurement using radial polarizer fabricated by direct atomic force microscope stroking method," Meas. Sci. Technol. **18**(6), 1673–1677 (2007).
14. Y. S. Changm P. Y. Chien and M. W. Chang, "Distance and velocity measurements by the use of an orthogonal Michelson Interferometer," Appl. Opt. **36**, 258–264 (2008).
15. G. M. Lerman, U. Levy, "Generation of a radially polarized light beam using space-variant subwavelength gratings at 1064 nm," Opt. Lett. **33**(23), 2782–2784 (2008).

1. Introduction

Vector beams, are the subject of extensive study over the last few years due to their special features such as a tight focal spot and strong longitudinal component of the electric field at the focal plane [1–7]. The spatially varying polarization direction of these beams can be used for gaining information that is not accessible with spatially homogenous polarization fields such

#118033 - $15.00 USD Received 1 Oct 2009; revised 16 Nov 2009; accepted 18 Nov 2009; published 3 Dec 2009

as the linear and circular polarizations [8–11]. For example, a Mach – Zehnder interferometer operating with radial polarization was demonstrated for the measurement of the geometric phase [12], and a radial polarizer was shown to be useful for a single shot birefringence measurement [13].

Typically, interferometry is performed with two beams having the same polarization; nevertheless, interferometry of orthogonally polarized beams was demonstrated for various applications, e.g. distance and velocity measurements [14]. In this paper we propose a new interferometric set-up, coined the radial polarization interferometer (RPI), which combines the concepts of spatially inhomogeneous polarization fields and orthogonal polarization interferometry. The RPI generates a spatially varying intensity pattern along the cross section of the beam, assisting in overcoming the limited accuracy enforced by the bit quantization of a CCD camera. Using the RPI, we found that it is possible to measure smaller phase changes compared with conventional Michelson interferometer (CMI). The paper is structured as follows: section 2 provides the description of the RPI apparatus and its operation principle. In section 3 an analytic expression is developed for the intensity distribution of the RPI and several examples are given. Section 4 describes a phase measurement experiment with the RPI, while section 5 describes a distance measurement experiment with the RPI using a tunable laser source. In section 6 a comparison between the RPI and the CMI is given and some case studies are discussed.

2. Apparatus and operation principle of the RPI

A schematic diagram of the proposed RPI is shown in Fig. 1. It is based on a modified version of the Michelson interferometer. A laser beam that is linearly polarized along the x axis, passes through a half wave plate oriented with its optical axis at 22.5° with respect to the incident polarization direction, thus rotating the polarization at 45° with respect to the x axis. The beam is next split into two beams with orthogonal linear polarizations by a polarizing beam splitter (PBS). Each of these beams passes through a quarter wave plate (QWP) oriented at 45° with respect to its polarization axis, and reflected back from a mirror (one mirror is moveable to generate a phase difference between the two arms) towards the QWP and the PBS. As a result two spatially overlapping beams that are linearly and orthogonally polarized with respect to each other are obtained. The beams then pass through a polarization conversion element that converts the two orthogonally linearly polarized beams into radially and azimuthally polarized beams. More details about the operation of this polarization conversion element are given in [15]. The two orthogonally, spatially varying polarized beams, pass through a linear polarizer serving as an analyzer. The plane of the analyzer is imaged to a CCD camera.

The electric field before the analyzer is the vector sum of the two fields in the two interferometer's arms, and similarly to the radial and azimuthal polarizations that constitute it, has a spatially varying polarization. Therefore, the imaged intensity distribution will have dark and bright areas, depending on the local projection of the polarization field on the analyzer. Clearly, phase difference between the two arms of the interferometer will modify the vector sum of the two beams, resulting in a modulation of the spatially varying intensity distribution behind the analyzer. We next cast this explanation in mathematical form.

#118033 - $15.00 USD Received 1 Oct 2009; revised 16 Nov 2009; accepted 18 Nov 2009; published 3 Dec 2009

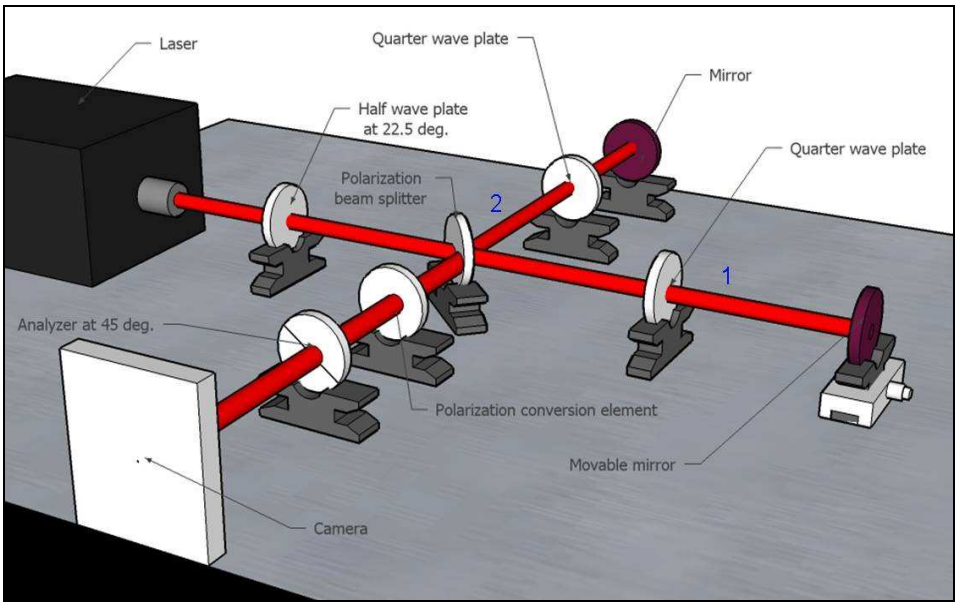

Fig. 1. Schematic representation of the RPI.

3. Theory of the RPI

The normalized intensity distribution of a CMI is given by:

$$I_1(\phi) = \frac{1}{2}(1+\cos\phi) \tag{1}$$

Where φ is the phase difference between the interferometer's arms. The normalized intensity distribution of the RPI is given by

$$I_2(\phi,\theta,\phi_p) \propto \left| T_p \cdot (V_r e^{i\phi} + V_a) \right|^2 \tag{2}$$

Where $V_r = \begin{pmatrix} \cos\theta \\ \sin\theta \end{pmatrix}$ and $V_a = \begin{pmatrix} -\sin\theta \\ \cos\theta \end{pmatrix}$ are the Jones vectors of the radial and azimuthal polarizations, respectively, $T_p = \begin{pmatrix} \cos^2\phi_p & \sin\phi_p\cos\phi_p \\ \sin\phi_p\cos\phi_p & \sin^2\phi_p \end{pmatrix}$ is the Jones matrix of a linear polarizer, φ is the phase difference between the interferometer's arms, θ is the azimuthal angle of a specific coordinate at the beams cross section and φ_p is the angle of the optical axis of the polarizer. Using these expressions we obtain

$$I_2(\phi,\theta,\phi_p) = \frac{1}{2}(1+\sin(2(\phi_p-\theta))\cdot\cos\phi) \tag{3}$$

By setting $\varphi_p = \pi/4$ this expression becomes

$$I_2(\phi,\theta) = \frac{1}{2}(1+\cos 2\theta\cdot\cos\phi) \tag{4}$$

#118033 - $15.00 USD Received 1 Oct 2009; revised 16 Nov 2009; accepted 18 Nov 2009; published 3 Dec 2009

Figure 2 schematically shows the polarization direction of the superpositioned beam before the analyzer for several values of phase difference between the interferometer's arms (upper panel). For each of these cases, the simulated intensity distribution after the analyzer as expected to be captured by the CCD camera is shown as well (lower panel). It can be seen that changing the phase difference between the arms by π results in a 90° rotation of the intensity distribution. More importantly, the intensity difference between maximum and minimum intensity is also changing with the phase difference.

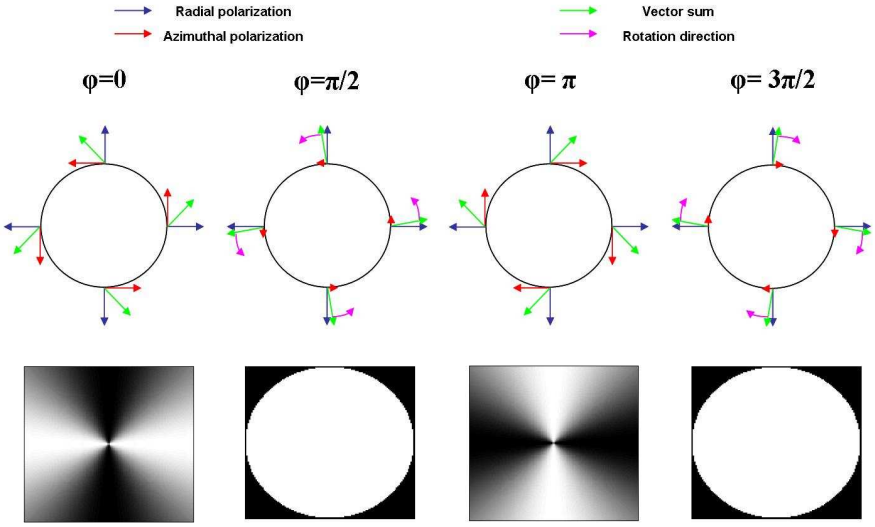

Fig. 2. Schematic representation of the polarization fields before the analyzer for a few values of ϕ. The vector sum (green arrows) of the radial (blue arrow) and azimuthal (red arrows) is shown for each case. the rotation direction is shown as well (purple arrows) when the field has a circular polarization. Simulated intensity distribution after the analyzer is shown for each case. White color represents high intensity.

We track this intensity difference by defining the contrast of the interferogram as $C = \frac{\max(I(\theta)) - \min(I(\theta))}{\max(I(\theta)) + \min(I(\theta))}$, where $I(\theta)$ is the intensity as a function of θ, calculated from the interferogram's data. From the analytical expression (Eq. (4) and from Fig. 2, one can notice that the contrast is changing from 1 to 0 and back to 1 upon varying the phase difference by π. At the same time, the orientation of the pattern is rotated by $\pi/2$, giving another valuable information for determining the phase.

4. Phase measurement

To demonstrate the effects discussed above, we built the RPI shown in Fig. 1 and used it to measure phase differences. The illumination source is an Nd:YAG laser operating at 1064 nm wavelength. The phase difference between the interferometer's arms was altered in small increments by inserting a ~0.24 mm thick glass plate into one of the interferometer's arms and rotating it in small steps of 0.15 degrees which is equivalent to an average phase change of 0.35 radians. For each phase value the intensity distribution behind the analyzer was captured by a CCD. Figures 3(a)-3(d) shows representative examples of the intensity distribution recorded by the CCD camera. Figures 3(a) and 3(b) shows the intensity distributions as obtained separately from arms 1 and 2 of the interferometer. The interference patterns for a phase difference of 0 and π between the two interferometer's arms are shown in Figs. 3(c) and 3(d), respectively, with the polarizer oriented at $\pi/4$ with respect to the x axis.

#118033 - $15.00 USD Received 1 Oct 2009; revised 16 Nov 2009; accepted 18 Nov 2009; published 3 Dec 2009

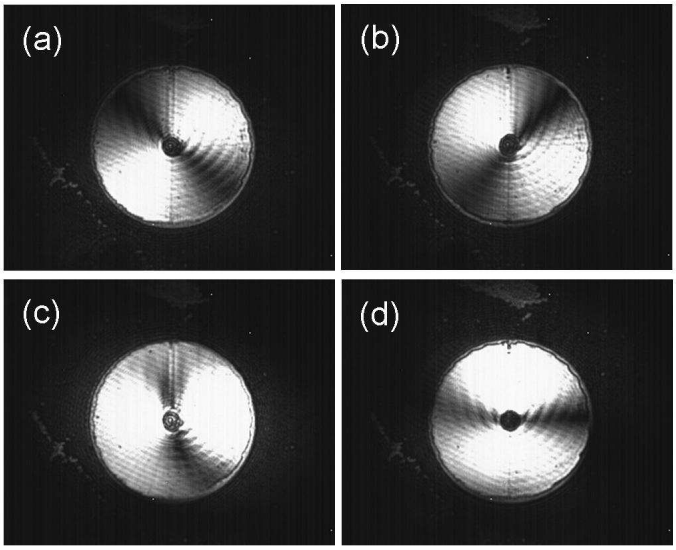

Fig. 3. Representative intensity distribution after passing through the analyzer: (a, b) separate intensity distribution as obtained from arms 1 and 2 respectively. (c, d) interference pattern of the two arms with 0 and π phase difference between them, respectively.

From each of the interference patterns, captured at different phase difference between the interferometer's arms we calculated the intensity as a function of the azimuthal angle θ by integrating the intensity along the radial coordinate for each value of θ. Figure 4 shows the calculated intensity as a function of the phase difference ϕ and the azimuthal angle θ. The theoretical intensity distribution as expressed in Eq. (4) is shown as well for comparison.

#118033 - $15.00 USD Received 1 Oct 2009; revised 16 Nov 2009; accepted 18 Nov 2009; published 3 Dec 2009

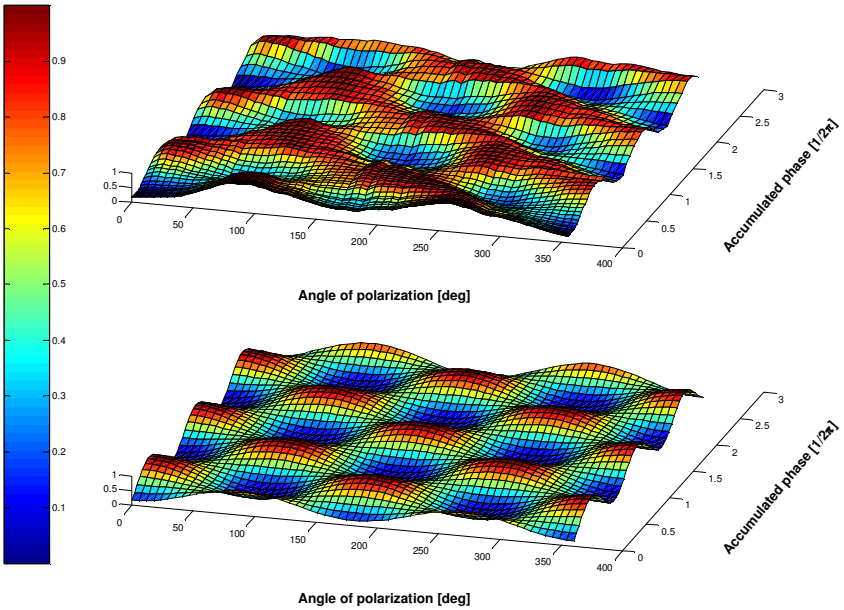

Fig. 4. Intensity as a function of the azimuthal angle and the phase difference between the interferometer's arms. The experimental results (upper panel) were calculated from each interferogram by integration along the radial coordinate. The theoretical intensity distribution is shown as well for comparison (lower panel). The accumulated phase is measured relative to an arbitrary reference point.

As can be seen, the intensity maxima are rotated by $\pi/2$ in azimuthal angle θ upon changing the phase difference between the interferometer's arms by π. These results clearly show the vectorial nature of the interferometer and the periodicity of π in the contrast of the interferogram. From each interferogram captured at a different phase value, we calculated the contrast and plot it against the phase difference between the interferometer's arms. The results are shown in Fig. 5. One can clearly observe the periodicity of π in phase difference, as expected. Unfortunately, the obtained contrast is limited. This is attributed to imperfections in the radial polarization conversion element and to a small translation of one beam with respect to the other due to the rotation of the glass plate.

#118033 - $15.00 USD Received 1 Oct 2009; revised 16 Nov 2009; accepted 18 Nov 2009; published 3 Dec 2009

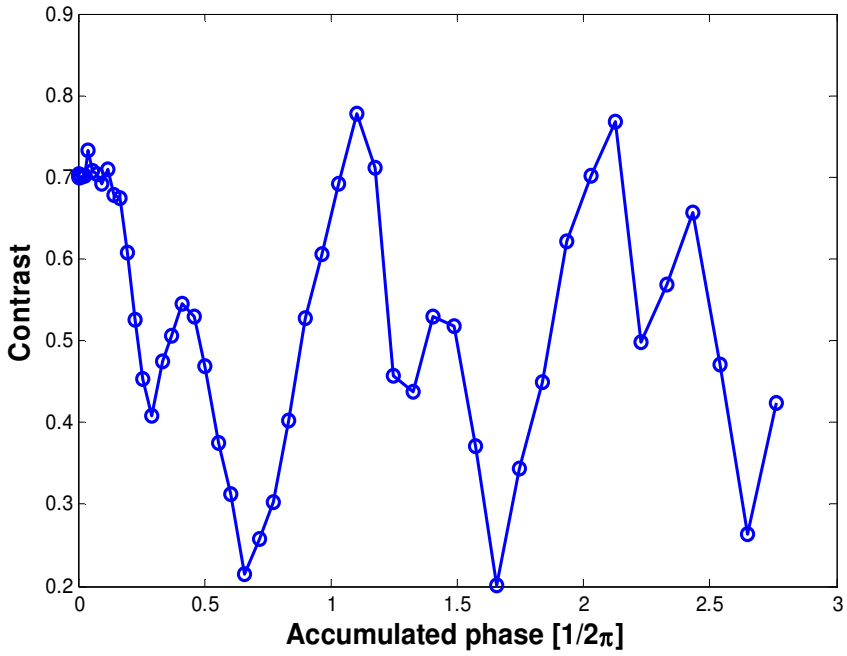

Fig. 5. Contrast of interferograms as a function of the accumulated phase difference.

5. Distance measurement

Another form of using the RPI is by keeping the mirrors constant and using a tunable wavelength illumination source to find the difference in path length between the two arms. The relative phase between the interferometer's arms is changing with wavelength, and the recorded interferogram varies accordingly, allowing us to find the relative path difference between the two arms. To qualitatively demonstrate this concept we used a tunable laser source (Velocity, New focus) with wavelength range of 960-995 and recorded the interferograms while scanning the illumination wavelength. Figure 6 shows the obtained intensity as a function of the polarization angle θ and the illumination wavelength, in the range of 980-981 nm, with resolution of 0.01 nm.

#118033 - $15.00 USD Received 1 Oct 2009; revised 16 Nov 2009; accepted 18 Nov 2009; published 3 Dec 2009

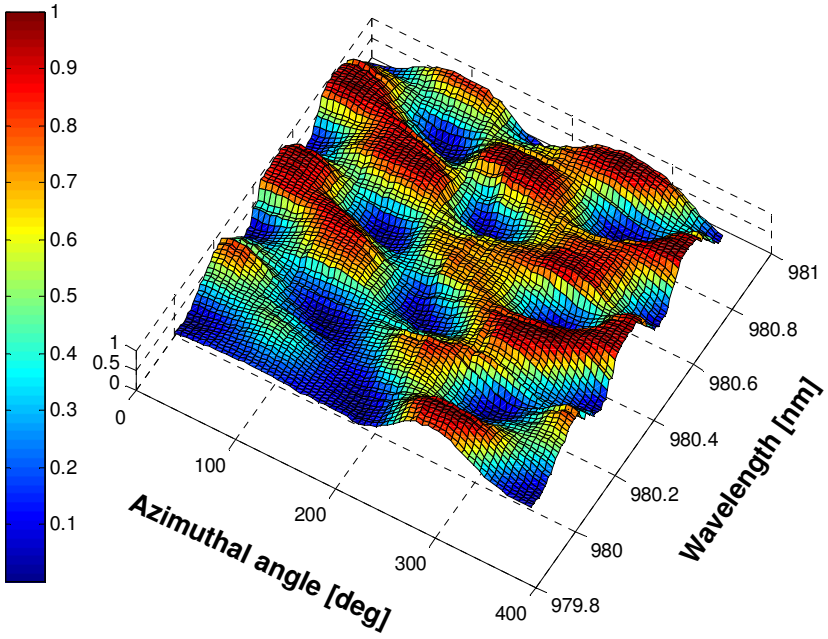

Fig. 6. Intensity as a function of the azimuthal angle and the illumination wavelength.

As in the previous section, maxima rotation of $\pi/2$ in the azimuthal angle θ occurs as the variation in illumination wavelength corresponds to a π phase change between the interferometer's arms. Similarly to the previous case, the contrast is expected to vary as the wavelength is scanned, because of the variation in phase difference between the two arms. This effect is demonstrated in Fig. 7 where we plot the contrast of the interferograms as a function of the illumination wavelength.

#118033 - $15.00 USD Received 1 Oct 2009; revised 16 Nov 2009; accepted 18 Nov 2009; published 3 Dec 2009

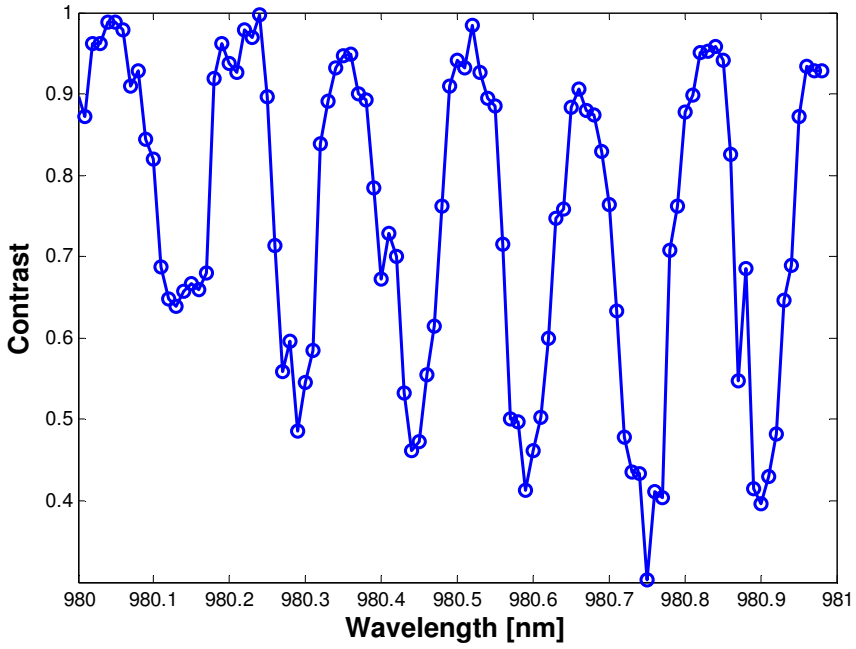

Fig. 7. Contrast of the interferograms as a function of the illumination wavelength. The contrast has a period of π where each maximum in the contrast plot has an intensity distribution that is 90° rotated with respect to the adjacent maxima.

The contrast maxima are obtained when the phase difference between the two arms is an integer multiplication of π according to $\frac{2 \cdot \Delta L}{c} \omega = m\pi$, where ΔL is the path difference between the interferometer's arms, c is the speed of light, ω is the angular frequency of the illumination light and m is an integer. A plot of the phase of the maxima as a function of the angular frequency of the illumination light is shown in Fig. 8. From the slope of this linear curve, one can calculate ΔL, and using the above results we found that $\Delta L = 1.56 \pm 0.03 mm$. The accuracy of this measurement can be improved by improving the quality of the radial polarization converter (originally optimized for 1.064 micron wavelength).

#118033 - $15.00 USD Received 1 Oct 2009; revised 16 Nov 2009; accepted 18 Nov 2009; published 3 Dec 2009

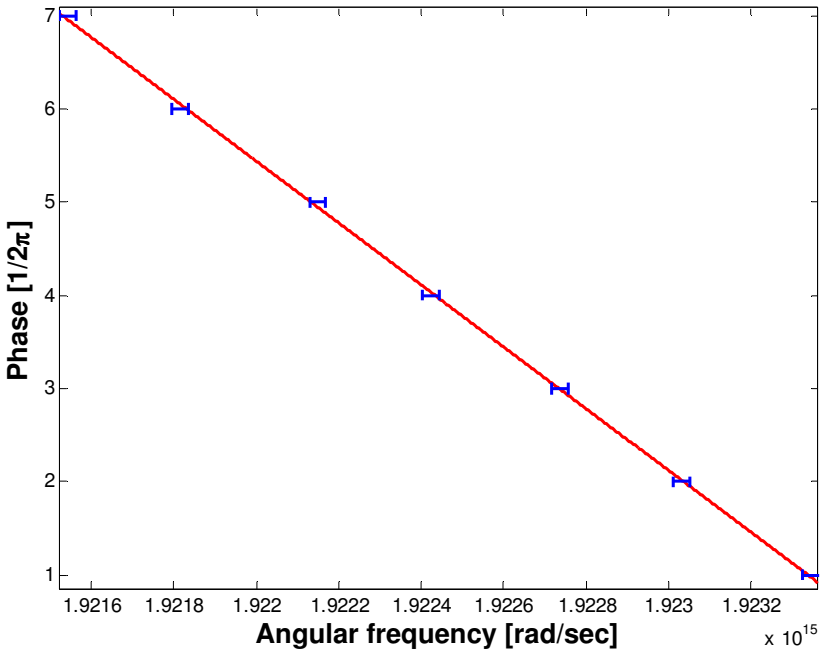

Fig. 8. Phase difference (relative to a reference value) as a function of the angular frequency of all the maximum points shown in Fig. 7. a linear fit is shown as well.

6. Comparison between the RPI and the CMI

The optical setup constructing the RPI is a bit more complicated than that of the CMI, because it requires a camera for its operation as opposed to CMI that can operate with a single detector. In addition, the two beams need to be well aligned such that their centers coincide. Nevertheless, the RPI provides valuable spatial information that can be used to measure phase changes with higher accuracy compared with the CMI. In displacement measuring interferometry, the displacement of the mirror modifies the phase difference between the interferometer's arms resulting in an intensity change on the detector. In practice, a digitized detector with a finite number of bits is typically used. Therefore, neglecting all error sources except the quantization error, the detection resolution of phase changes is limited by the least significant bit (LSB). For example, by taking the derivative of Eq. (1) and assuming $\varphi = \pi / 4$, the minimum detectable phase change is given by $\Delta\phi_{\min} = 2\sqrt{2}\Delta I_{\min}$,where $\Delta I_{\min}$ is the minimal detectable intensity change. Assuming a 10 bit detector, $\Delta\phi_{\min} \approx 3 \cdot 10^{-3}\, rad$.

In contrast, for a given phase difference φ the intensity distribution on the camera of the RPI, is not uniform. Instead it is spatially varying according to Eq. (4) with a range of $2\cos\phi$ across all the pixels of the camera. Therefore, it is very likely to find pixels with intensity that is very close to the next gray level so that even a slight phase change, much below the LSB is expected to modify the intensity reading in those pixels. Using Eqs. (1) and (4) we calculated the minimum detectable phase change for the RPI and CMI as a function of the phase difference φ between the arms. A change in phase difference is assumed to be detectable if the intensity measured by the camera is modified in at least 100 of its pixels. The minimum detectable phase change of the RPI was found to be always smaller than that of the CMI. The

#118033 - $15.00 USD Received 1 Oct 2009; revised 16 Nov 2009; accepted 18 Nov 2009; published 3 Dec 2009

calculated ratio of the minimum detectable phase change in the CMI and the RPI is shown in Fig. 9 as a function of the phase difference ϕ on a semi log scale. This calculation assumes a CCD with 16 bits quantization and 1024x1024 pixels.

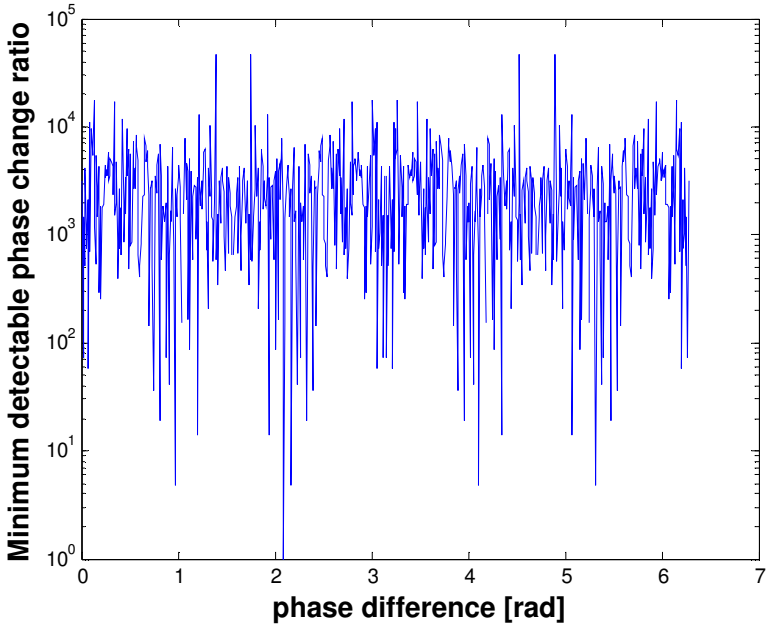

Fig. 9. Ratio of the minimal detectable phase change in a CMI and the RPI as a function of the phase difference between the interferometer's arms.

As evident by this case study, the minimum detectable phase change in the RPI is, on average, 3-4 orders of magnitude smaller compared with the Michelson interferometer, thus allowing the measurement of much smaller displacements. This ratio increases with the increase in the number of pixels in the camera.

In the previous analysis, we ignored all noise sources except quantization noise (i.e. limited number of bits per pixel). In practice, additional noise sources may impose a limit to the improvement achievable by the proposed approach. An accurate calculation of the device performances needs to be done per each given application when all noise sources are known and being taken into account. While such an analysis is beyond the scope of this paper, we next describe a specific example where other noise sources are also included. We assume an 8 bit camera with 1024x1024 pixels and compared the performance of the two interferometers (i.e. how close their phase change reading to the accurate phase change value) in the presence of a random noise source. In order to perform the comparison, for each phase difference φ we added a phase step which is equivalent to 1/16 LSB plus a random noise and generated the resulting intensity pattern. Using Eqs. (1) and (4) and the intensity change in each pixel, we retrieved the phase change reading of each pixel, and averaged on all pixels to get the final phase change reading of the interferometer. Figures 10(a) and 10(b) shows the phase change reading of the two interferometers as a function of the phase difference between the interferometer's arms for noise amplitudes of 1 and 0.1 LSB, respectively. The actual phase change value is shown as well for reference. As can be seen, for most phase difference values the accuracy of the RPI is much better than the CMI. When a noise of 1 LSB is assumed, the error of the RPI is smaller than that of the CMI in 67% of the cases. Within this range the average RPI error is 7.46 times smaller than that of the CMI. In the remaining 33%, the error of the CMI is smaller than that of the RPI, although only by an average factor of 3.71. When a

#118033 - $15.00 USD Received 1 Oct 2009; revised 16 Nov 2009; accepted 18 Nov 2009; published 3 Dec 2009

noise of 0.1 LSB is assumed, the results of the RPI improve providing smaller error in 92% of the cases. Within this range the average RPI error is 12.31 times smaller than that of the CMI., In the remaining 8%, the error of the CMI is smaller than that of the RPI, although only by an average factor of 1.56 Moreover, the error of the RPI is systematic, and thus can be pre-compensated, while the phase reading of the CMI oscillates sharply, making the pre-compensation more challenging.

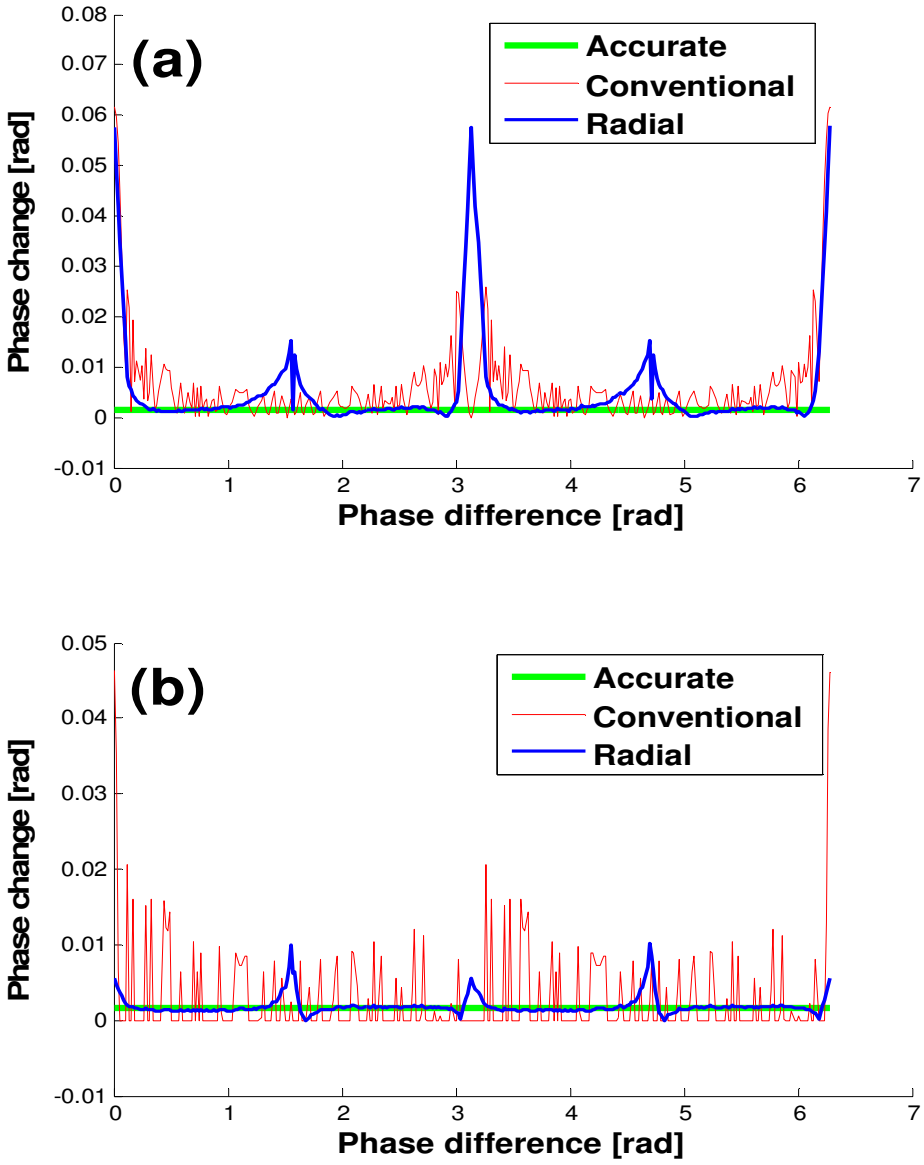

Fig. 10. phase change reading of the two interferometers as a function of the phase difference between the interferometer's arms. (a) Noise amplitudes of 1 LSB. (b) Noise amplitudes of 0.1 LSB. The accurate phase change value is shown as well for reference (green).

While the RPI is mostly promising for translation measurements, it can also be used for retrieving the phase profile of a test object that is inserted into one of the interferometer's arms. To demonstrate this capability we simulated a case study in which a lens with a circular symmetric quadratic phase profile is inserted into one of the arms of the RPI. Figure 11 shows

#118033 - $15.00 USD Received 1 Oct 2009; revised 16 Nov 2009; accepted 18 Nov 2009; published 3 Dec 2009

the interferograms generated by the CMI (left) and the RPI (right). It can be seen that the RPI interferogram has the same number of fringes as that of the CMI. Nevertheless, while the CMI fringes exhibit constant intensity along the azimuthal direction, the RPI fringes exhibit alternating intensity pattern along the azimuthal direction, following the $\cos(2\theta)$ dependency (Eq. (4). As a result, the paths along $\theta = 0$ and $\theta = 90^0$ are flipped in their intensities. Therefore, by considering both paths for reconstructing the phase profile, it is possible to find an intensity minimum every π phase shift along the radial coordinate, compare with the CMI where minimum intensity is obtained every 2π along the radial coordinate. This fact may be helpful in reconstructing the phase profile of the test object. This is because the detection of a small intensity change in a shot noise limited system is more accurate in the vicinity of a minimum than in the vicinity of a maximum, owing to the lower noise level.

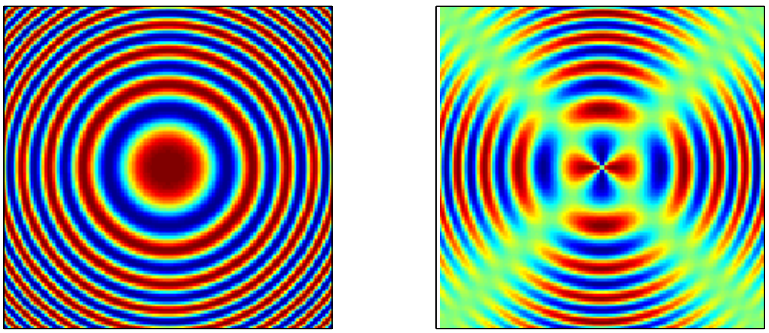

Fig. 11. Interferograms generated by the CMI (left) and the RPI (right) when a lens with a circular symmetric quadratic phase profile is inserted into one of the interferometer's arms.

7. Summary and conclusions

In summary, we analytically and experimentally demonstrated a new type of interferometric measurement combining the concepts of spatially inhomogeneous polarization fields and orthogonal polarization interferometry. By interfering radially and azimuthally polarized beams, the phase difference between the interferometer's arms is manifested as spatially varying intensity distribution. This is in contrast with conventional interferometers where phase change results in a spatially uniform intensity change. This unique method provides additional spatial information that can be used for displacement and phase change measurements with improved accuracy compared with a CMI.

Acknowledgements

The authors thank Nissim Ben Yosef for fruitful discussions, and acknowledge the partial financial support of the Israeli Science Foundation, and the Peter Brojde Center for Innovative Engineering and Computer Science. G. M. Lerman acknowledges financial support by the Eshkol fellowship of the Israeli Ministry of Science and Culture.

#118033 - $15.00 USD Received 1 Oct 2009; revised 16 Nov 2009; accepted 18 Nov 2009; published 3 Dec 2009